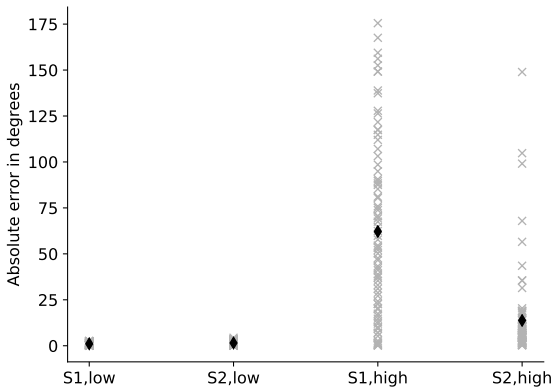

Figure S1. Absolute error in direction decoding in the RO ring at difference noise level. Related to Figure 2

S1 and S2 correspond to Scenarios I and II respectively. Low refers to reference noise level $\sigma_n = 0.015$ and high refers to higher noise level $\sigma_n = 0.03$. For each condition, 5 trials for every target direction were performed so there were 80 trials in total (marked with gray crosses). The black diamond indicates the mean for each condition. The network model in Scenario II is more robust to noise due to the between-ring coupling.

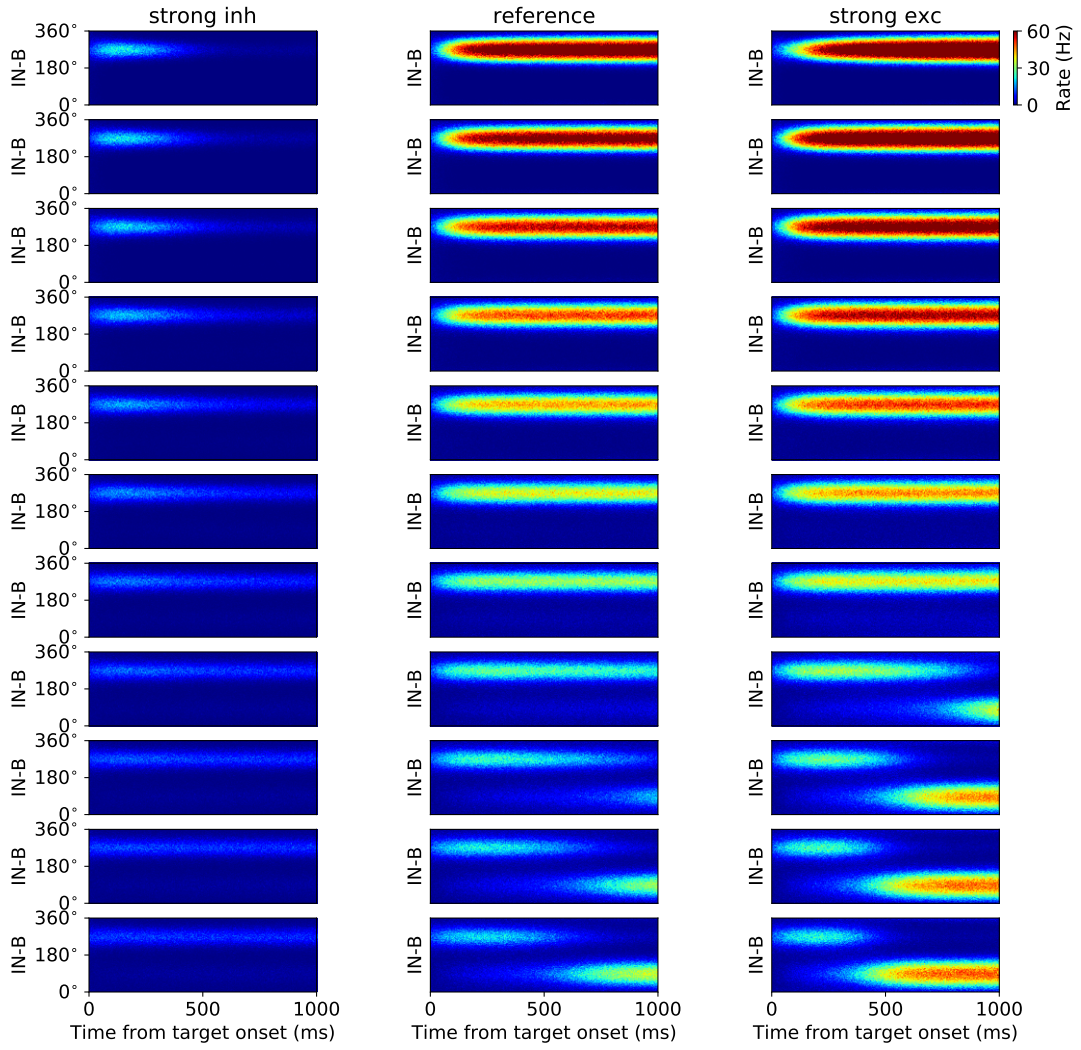

Figure S2. Spatiotemporal activity pattern of IN-B population of the circuit model when the chosen target is A, presented at 90°. Related to Figure 2

From left to right, three conditions in Figure 2 E are considered: strong inhibition ($J_- = -0.6$ nA, $J_+ = 1.9$ nA), reference ($J_- = -0.35$ nA, $J_+ = 1.9$ nA) and strong excitation ($J_- = -0.35$ nA, $J_+ = 2.02$ nA). From top to bottom, the value of α increases from 0 to 1 in step of 0.1.

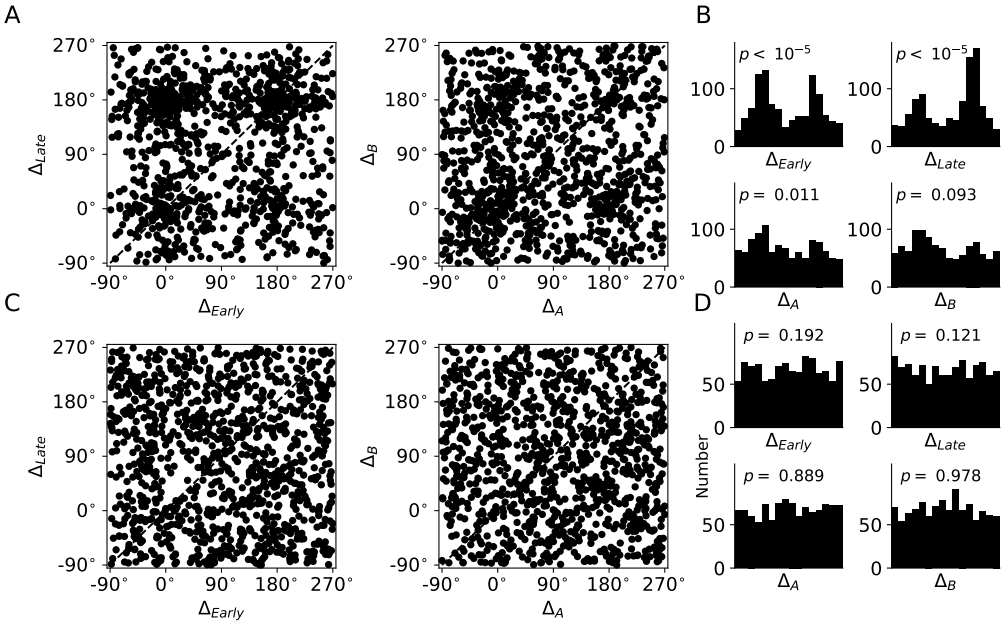

Figure S3. Representation of all recorded neurons in comparison with random tuning curves. Related to Figure 5

(A) Representation of all recorded neurons in the space of peak differences.

(B) Histograms of neuron count for each dimension. The p-values indicate the significance of dip test.

(C) For comparison, 1078 pairs of randomly generated tuning curves with firing rate values drawn from a uniform distribution were generated and represented in the 4-dimensional space of peak differences.

(D) Histograms of the neuron count for each dimension of peak-difference. The p-values represent the significance of the dip test.

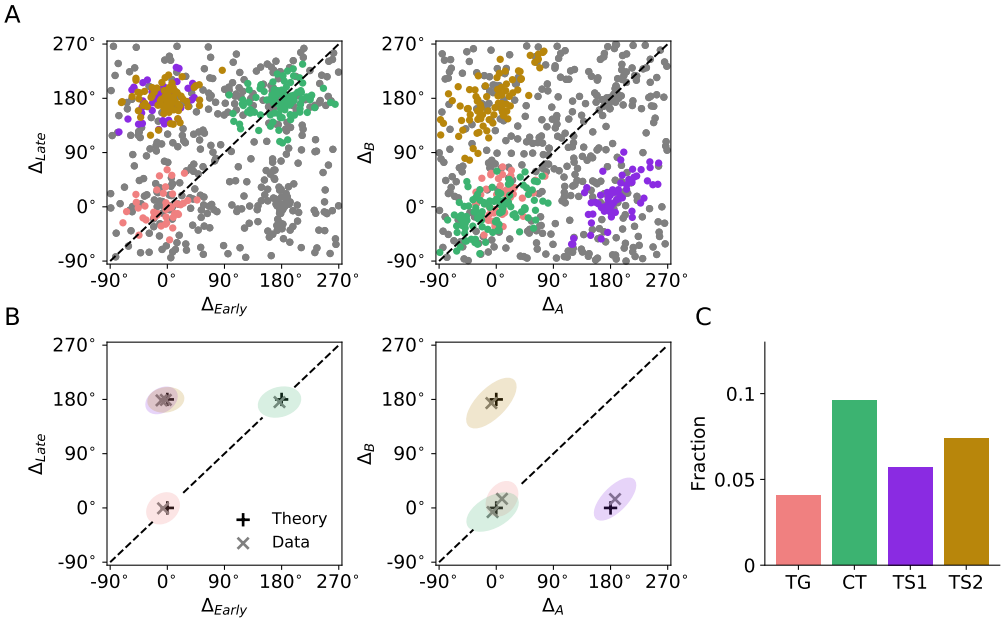

Figure S4. LPFC neuron type classification using stricter classification criteria. Related to Figure 5

Same as Figures 5C, E and F but the clustering analysis was performed with stricter criteria ($\epsilon = 55°$).

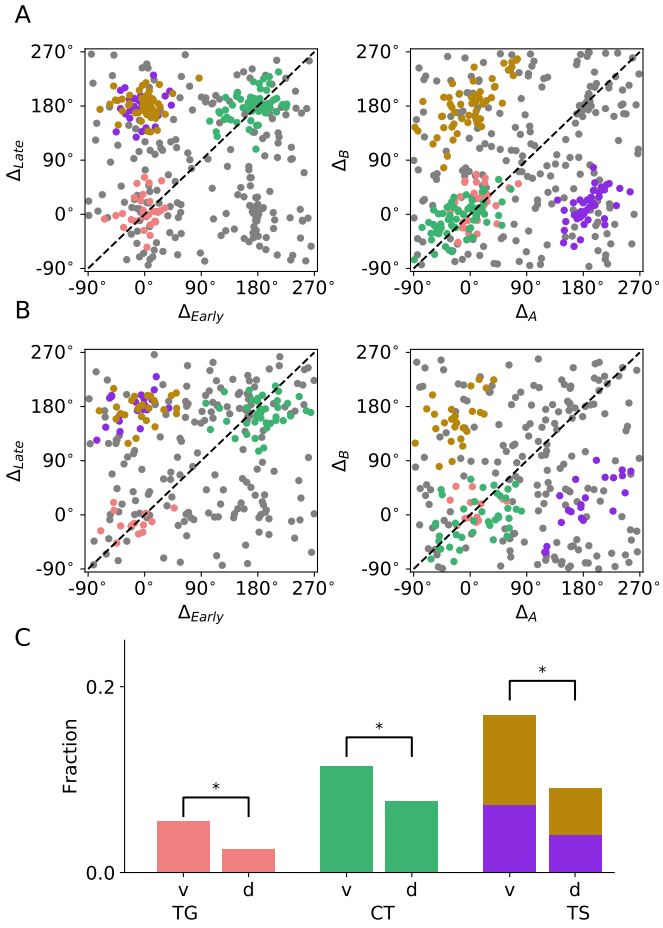

Figure S5. Comparison of neuron type classification between LPFCv and LPFCd using stricter classification criteria. Related to Figure 6

All spatially selective neurons in Figure S4A were plotted separately for LPFCv and LPFCd.

(A) Representation of LPFCv neurons in the space of peak differences.

(B) Representation of LPFCd neurons in the space of peak differences.

(C) Fraction of different types of neurons among spatially selective ones in LPFCv and LPFCd. Asterisks indicate $p < 0.05$ (two-sample t-test).

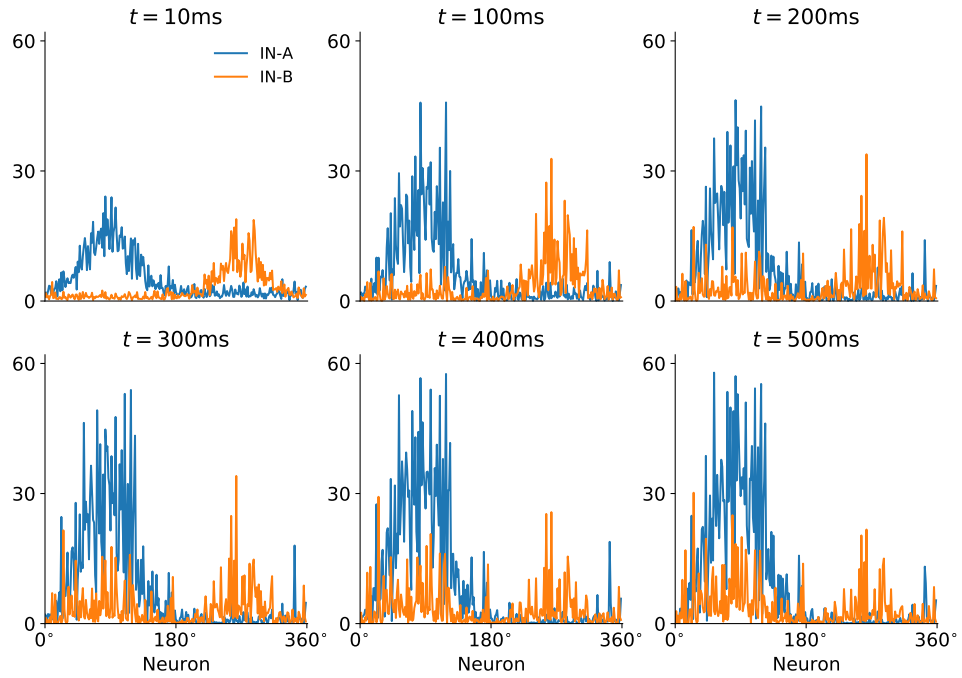

Figure S6. Snapshots of the activity profiles of IN-A and IN-B rings in a model simulation. Related to Figure 7

Snapshots of IN rings' activity in Figure 7 are taken at 10, 100, 200, 300, 400 and 500 ms after target onset. Here A is the chosen target. At t =10 ms, the activity profiles of the two IN rings peak at their respective target location. As time evolves, the activity bump in the IN-A ring grows to a steady value, whereas the IN-B ring has two bumps: the original bump is maintained and another emerges at the chosen target location.

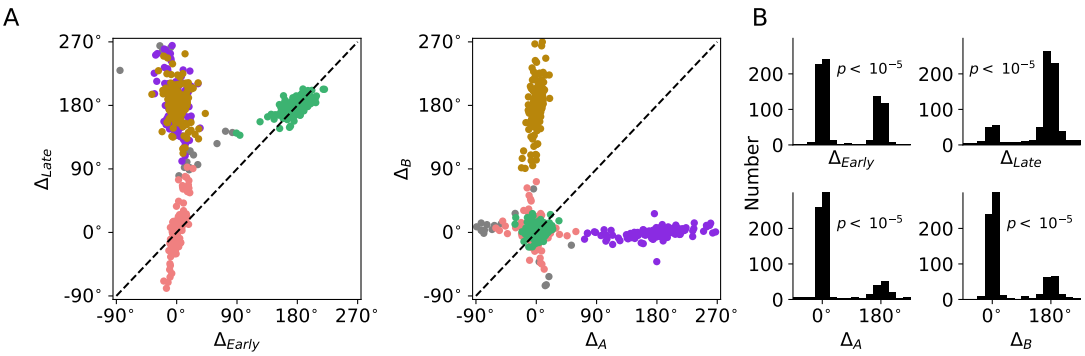

Figure S7. Classification of neurons from a model simulation with heterogeneous interactions. Related to Figure 7

(A) Representation of simulated neurons in the space of peak-difference. The clusters were identified with DBSCAN. Different clusters were represented by different colors with gray as unclassified.

(B) Histograms of spatially selective neurons for each dimension of peak-difference.

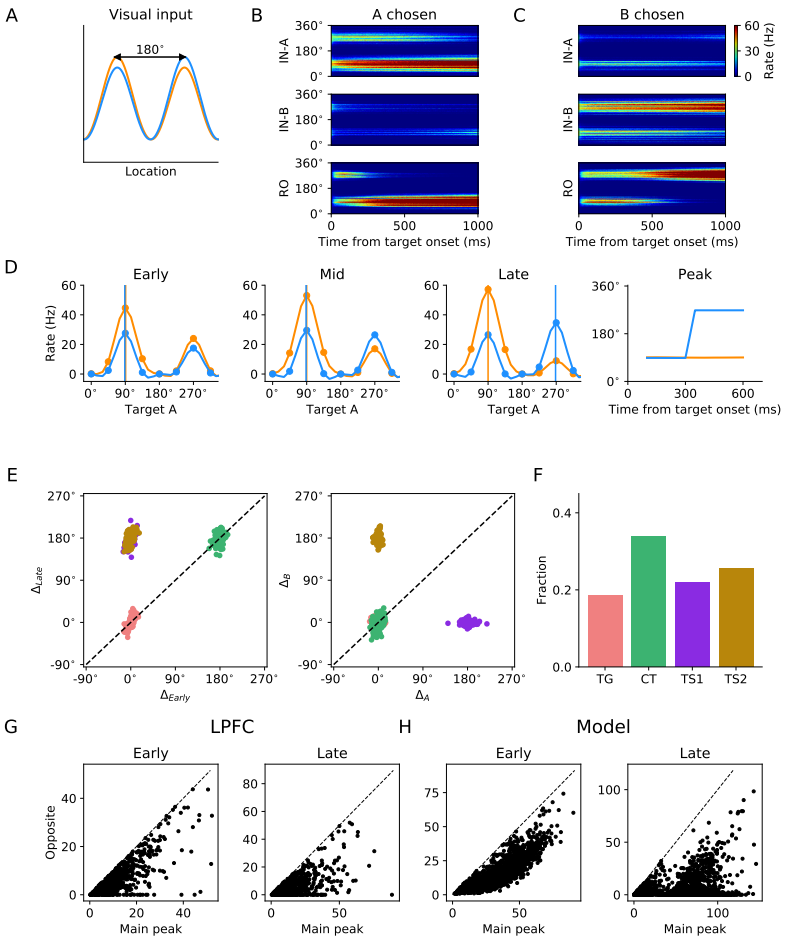

Figure S8. Model neurons in response to bimodal visual input. Related to Figure 7
(A) The visual input is presented as a Gaussian-profiled current which has a major peak at the direction of its target cue and a smaller peak at the direction of the other target cue, located at the opposite direction (compared with Figure 1D).
(B) Activity of model neurons when target A which appeared at 90° was chosen.
(C) Activity of model neurons when target B which appeared at 270° was chosen.
(D) Spatial tuning curves and time evolution of their peak location of a TS neuron. The tuning curves were constructed by cubic spline interpolation.
(E) Representation of neuron clusters in peak-difference space. Each ellipse represents one SEM of one cluster. Black pluses indicate theoretically predicted locations of peak differences for different neuron types, while gray crosses denote the mean for each cluster, or the center of the ellipse.
(F) Fraction of different neuron types.
(G-H) Amplitude of the tuning curve at the direction opposite to the maximum versus the maximum for LPFC neurons (G) and model neurons (H). The black dashed line marks the diagonal.

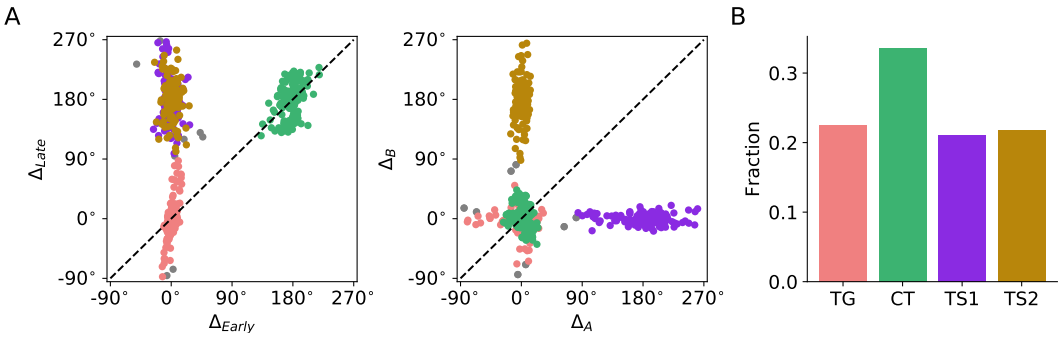

Figure S9. Effects of intrinsic neuronal heterogeneity on circuit properties. Related to Figure 8
Here neuronal heterogeneity is implemented by drawing two Gaussian-distributed parameters for each neuron. The two parameters are the baseline current and the standard deviation of the input noise, with the mean set to be the same as that of the homogeneous neurons. The standard deviation of the distribution κ is varied in the same fashion. Network heterogeneity strength β is set to be 2 nA.
(A) Representation of simulated neurons in the space of peak-difference at $\kappa = 0.025$. The clusters were identified with DBSCAN. Different clusters were represented by different colors with gray as unclassified.
(B) Number of different types of neurons.